Optics Communications 405 (2017) 372–377

Contents lists available at ScienceDirect

Optics Communications

journal homepage: www.elsevier.com/locate/optcom

Weighted wavefront reconstruction algorithm for multiple laser guide stars adaptive optics system

Chao Liu [a,b], Bin He [a,b], ZhaoLiang Cao [a,*], YuKun Wang [a,b], LiFa Hu [c], Li Xuan [a]

[a] State Key Laboratory of Applied Optics, Changchun Institute of Optics, Fine Mechanics and Physics, Chinese Academy of Sciences, Changchun, 130033, PR China
[b] University of Chinese Academy of Sciences, Beijing, 100039, PR China
[c] 3School of Science, Jiangnan University, Wuxi, 214122, PR China

ARTICLE INFO

Keywords:
Multi-LGSs
Wavefront reconstruction
Weighted method

ABSTRACT

We present a weighted method of wavefront reconstruction for multiple laser guide stars (LGS) adaptive optics (AO) system. Unlike simple averaging method in the traditional ground layer adaptive optics (GLAO), the weighted method generates different weighting factors according to LGSs' different positions for the reconstructed wavefront from different LGSs. And then the target aberration to correct could be obtained with summation of these wavefronts multiplied by their correspondent weighting factors. Wide-field simulations are presented and analyzed. Experiments in the lab are conducted to validate the method. The weighted method is better than the average method especially near the center area of FOV. At center of FOV, the SR is improved by about 0.2 compared to the average method and the SR decreases with enlargement of FOV. For the first time, the weighted wavefront reconstruction method effectively decreases the reconstruction error in multi-LGSs AO system. The simulation and experimental result show that weighted method is also promising to improve the imaging resolution of LGS adaptive optics systems in astronomical observations.

1. Introduction

Adaptive optics (AO) systems are widely used in astronomical optical telescopes to achieve high spatial resolution images [1–6]. AO needs to use relatively bright star to measure wavefront distortions introduced by turbulence [7]. To increase the very limited sky coverage of natural guide stars, laser guide star (LGS) is necessary and it had been demonstrated on Keck II telescope [8]. A single LGS will lead to the focal anisoplanatism error that is proportional to the pupil diameter of optical telescope. Its corrected field of view (FOV) is small and limited by angular anisoplanatism [9]. Therefore, to solve these problems, multiple laser guide stars are proposed [9]. In fact, many ground based telescopes were equipped with multiple LGSs, such as 6.5 m MMT and Gemini South Telescope [10–15]. All laser beacons are sensed independently, and then the aberration needed to be compensated is reconstructed from the individual measured results [12]. The more precise the reconstructed wavefront is, the better imaging quality of AO systems get.

The technique of multiple laser guide stars is very effective to improve wide-field imaging for large telescopes as demonstrated on MMT [12]. Ground layer AO (GLAO) was proposed for compensating the low altitude turbulence. Average method is used in GLAO technique that averaging the wavefronts of LGSs is treated as the target wavefront to be corrected. It is based on the assumption that atmospheric turbulence close to the ground is common to objects and every LGS beacons in the field of view. And aberration at higher altitude different for each beacon will be mitigated in the average [16,17]. As shown in Fig. 1, averaging the LGSs' wavefront is to find the common wavefront of LGSs, not to find the common wavefront of objects in large FOV. In the "gray zone", the common wavefront from LGSs and objects are different, which would cause most of residual anisoplanatism error for the conventional averaging the LGSs' wavefronts [16,17].

As shown in Fig. 1, the purple area are sensed separately by LGS1 and LGS2, which is the common aberration of objects, but not common for LGSs. To decrease the residual anisoplanatism error, our group presented the weighted wavefront reconstruction method to solve the problem. This method gives different weighting factor distributions based on the interpolation according to LGSs' relative positions rather than same weight factors as used in the conventional averaging method [18].

In this paper, the weighted wavefront reconstruction method is described in theory and validated experimentally in lab. In Section 2,

* Corresponding author.
E-mail address: caozlok@ciomp.ac.cn (Z. Cao).

http://dx.doi.org/10.1016/j.optcom.2017.08.032
Received 22 May 2017; Received in revised form 4 July 2017; Accepted 14 August 2017
Available online 6 September 2017
0030-4018/

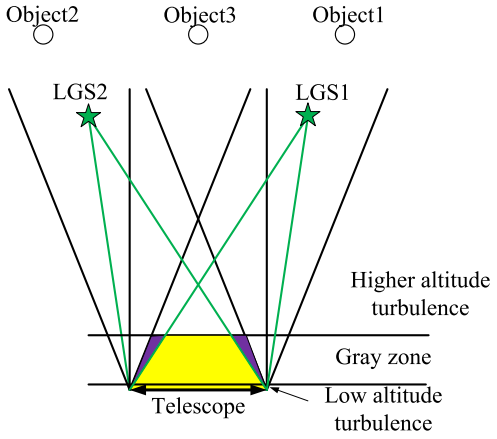

Fig. 1. Schematic diagram of turbulence paths for multiple LGSs AO.

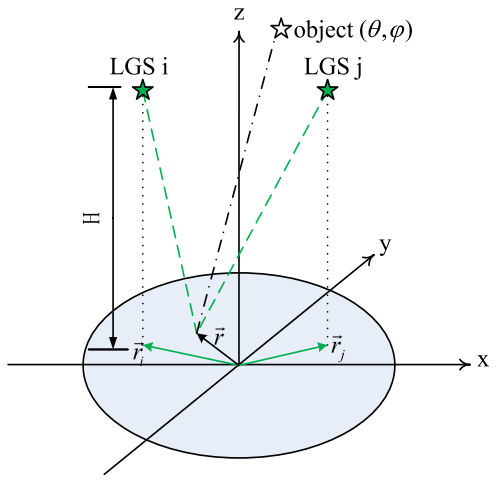

Fig. 2. Schematic diagram of LGSs' distribution and objective star with elevation angle θ and azimuth angle φ, light from LGS: dashed line; light from objective star: dot-dashed line.

the weighted wavefront reconstruction method for wide-field imaging is described for multiple LGS application. In Section 3, we simulated the performance under the used asterism of LGSs. In Section 4, the algorithm was tested experimentally in designed optical system in lab. Finally, conclusions were given in Section 5.

2. Theory of the weighted wavefront reconstruction

For wide-field imaging, the target wavefront to be corrected is the common wavefront along all directions in large FOV. The wide-field weighting factors are the average along all directions in the FOV. Firstly, the weighting factors along one direction are calculated by interpolation. Assume that n LGSs are projected at height H. $\boldsymbol{r}_i$ is the projected vector of the ith LGS on the telescope aperture as shown in Fig. 2.

A light beam (dashed line) from the ith LGS to the point $\boldsymbol{r}$ will passing through a point at the position $(\boldsymbol{r}-z\boldsymbol{r}/H+z\boldsymbol{r}_i/H, z)$. According to the near-field approximation, the aberrated wavefront of this LGS is calculated as:

$$\phi_i(\boldsymbol{r}) = \frac{2\pi}{\lambda}\int n\left[\frac{H-z}{H}\boldsymbol{r}+\frac{z}{H}\boldsymbol{r}_i, z\right]dz \tag{1}$$

where $n(\boldsymbol{r}, z)$ is the refractive index fluctuation along the beam at altitude z, and λ is the wavelength. $\boldsymbol{r}_i$ is the position vector of projected point of the ith LGS as shown in Fig. 2.

Table 1
Parameters for simulation.

Parameter	Value
Telescope's diameter	2 m
Number of LGSs	5
Central obscuration	0
Height of LGSs	10 km
LGSs asterism diameter	0.7 arcmin

The object wavefront present the wavefront along its direction. The turbulence aberrations from LGSs are different from that of object due to the different light propagation paths. The smaller the light propagation path differences are, the smaller the wavefront errors between the LGSs and the object are. So, it is reasonable that each LGS owns different weight factor distribution rather than same weight factor.

There is a linear relation between the object wavefront and LGSs' wavefronts as follows:

$$\widetilde{\phi}_o(r) = \sum_1^n k_i \times \phi_i \tag{2}$$

where k_i is the weighting factor. We wish to find the reasonable k_i that minimum the difference between the ideal values and estimated one. It should meet the unbiased estimation constraint:

$$\left\langle \sum_{i=1}^{n} k_i\phi_i - \phi_o \right\rangle = 0 \tag{3}$$

$$\sum_{i=1}^{n} k_i = 1, 0 \le k_i \le 1, (i = 1, 2, 3, \ldots, n). \tag{4}$$

To find the reasonable weighting factors k_i, we define J, the squared norm of the average difference between the target wavefront and their estimates as the following:

$$J = \left\langle \left(\sum_{i=1}^{n} k_i\phi_i - \phi_o \right)^2 \right\rangle. \tag{5}$$

We can get the following matrix equation by solving the J according to the Lagrange multiplier algorithm combined with Kolmogorov structure [18].

$$\begin{bmatrix} d_{11} & d_{12} & \cdots & d_{1n} & 1 \\ d_{21} & d_{22} & \cdots & d_{2n} & 1 \\ \vdots & \vdots & \ddots & \vdots & \vdots \\ d_{n1} & d_{n2} & \cdots & d_{nn} & 1 \\ 1 & 1 & \cdots & 1 & 0 \end{bmatrix} \begin{bmatrix} k_1 \\ k_2 \\ \vdots \\ k_n \\ \gamma \end{bmatrix} = \begin{bmatrix} d_{o1} \\ d_{o2} \\ \vdots \\ d_{on} \\ 1 \end{bmatrix} \tag{6}$$

where, $d_{ij} = |r_j - r_i|^{5/3}$ and $d_{oi} = |r_o + r - r_i|^{5/3}$. The weight factors k_i could be obtained by solving the matrix equation (6). The weighting factors depend on the location of the point $\boldsymbol{r}$, the direction along object and its corresponding projected vectors of LGS, $\boldsymbol{r_i}$, and are independent on C_n^2. Now we calculate weighting factors along one direction, and then wide-field weighting factors are calculated by averaging along all directions.

3. Simulation

In this section, we define an AO system with five Rayleigh LGSs as shown in Fig. 3. The relevant parameters for the AO system are given in Table 1 for simulation. The seven layers listed in Table 2 are used to model the turbulence [19]. The optimal number and position of LGSs are not discussed here. For simplification, the error of sensing the wavefronts is ignored, and the performance of AO system is only limited by the wavefront reconstruction algorithm here. The global tip-tilt component is sensed by NGS and irrelevant to the Strehl ratio (SR). So we only consider the error without tip-tilt.

According to the weighted wavefront reconstruction algorithm in Section 2, the calculated weighting factors of LGSs are shown in Fig. 3.

Table 2
Seven-layer turbulence profile used in simulation.

Height (m)	Strength	Wind speed (m/s)	Wind direction (°)
25	0.126	5.65	0.78
275	0.087	5.80	8.25
425	0.067	5.89	12.48
1 250	0.350	6.64	32.5
4 000	0.227	13.29	72.1
8 000	0.068	34.83	93.2
13 000	0.075	29.42	100.05

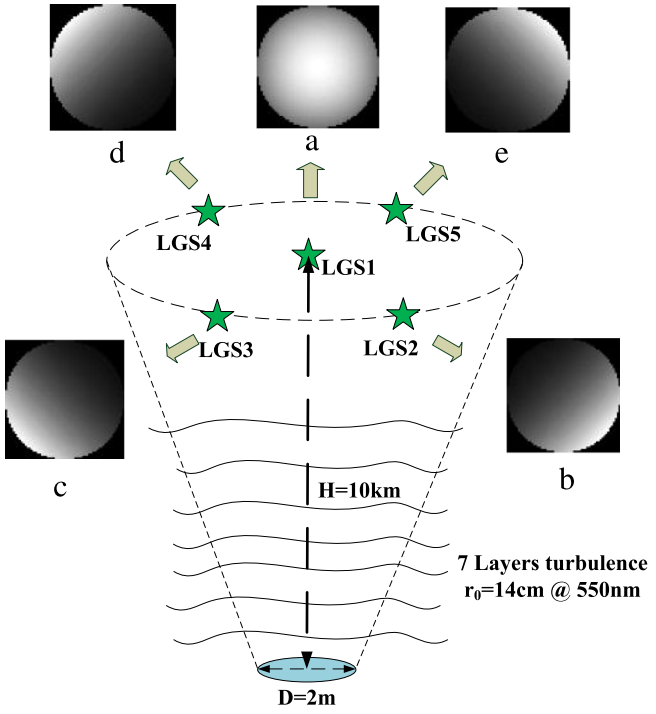

Fig. 3. Schematic diagram of AO for simulation and LGSs' weighting factors: telescope aperture 2 m; Atmosphere r_0 = 14 cm at 550 nm; Image (a)–(e) shows the obtained weighting factors distribution correspondent to LGS 1 to LGS 5.

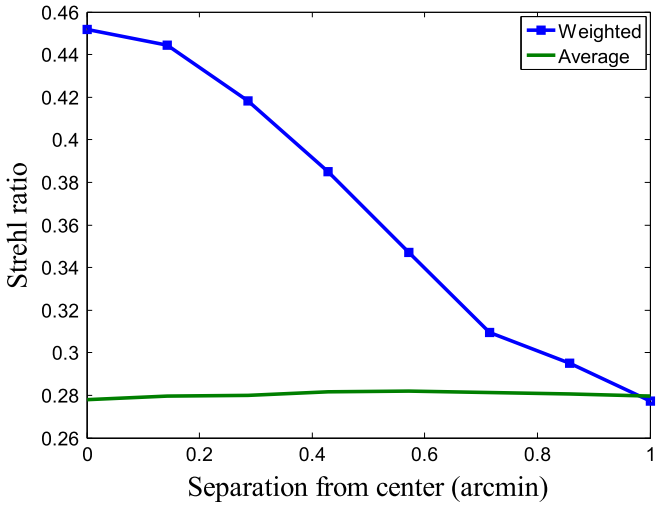

Fig. 4. Relationship between Strehl ratio with different methods and FOV.

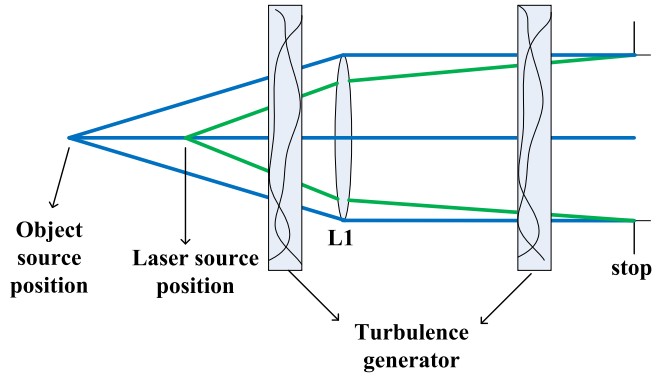

Fig. 5. Schematic diagram of two sources. (For interpretation of the references to color in this figure legend, the reader is referred to the web version of this article.)

The peak of weighting factors distribution of LGS1 is in the center, which means that the LGS1 contributes more than others in the center.

We calculate the wide-field weighting factors and obtain the SR in large FOV as shown in Fig. 4. The SR with average method is 0.28 within entire FOV, and the SR with weighted method is 0.45 at center area of FOV and decrease with enlargement of FOV. When the half of FOV is less than 1 arcmin, the weighted method is better than average method especially near the center area of FOV. At center of FOV, the SR is improved by about 0.2 compared to the average method. For low altitude turbulence, the averaging method and weighted method could reconstruct well. For "gray zone" turbulence, weighted method could reconstruct better. For high altitude turbulence, both methods would cause residual anisoplanatism error due to cone effect.

4. Experimental design

4.1. Source design and turbulence

LGSs are emulated at altitude of 10 km, which would cause cone effect. Two kinds of light sources are used in the optical layout, that is, object and laser sources as shown in Fig. 5. The object light emulates the light form infinity to measure the turbulence as reference. Light from object is collimated by lens L1 noted by the blue line in Fig. 5. In the experiment, we use turbulence generators to simulate two layers, one at altitude 600 m with r_0 = 16 cm, and the other at 8 km with r_0 = 30 cm. The stop is used to emulate the telescope pupil. However, the laser source not in the focus plane of lens L1 is used to emulate the Rayleigh LGS at an altitude of 10 km. Cone laser beam arrives at the field stop noted by the green line in Fig. 5. Five fiber laser sources were used to emulate five Rayleigh LGSs in 0.7 arcmin FOV in experiment as shown in Fig. 6.

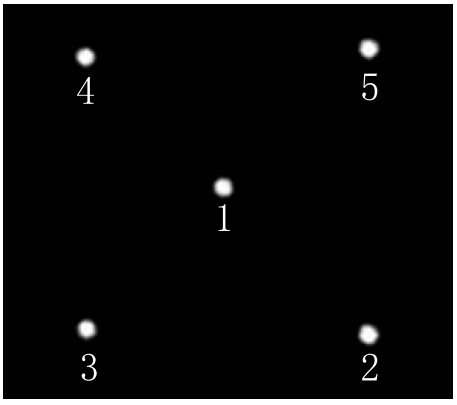

Fig. 6. Asterism of five fibers to emulate LGSs.

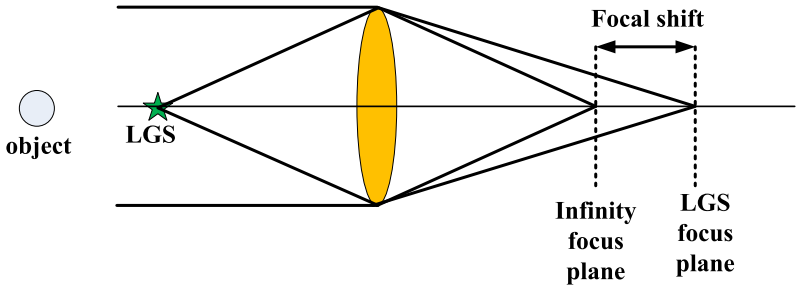

Fig. 7. Focal shift between object and LGS.

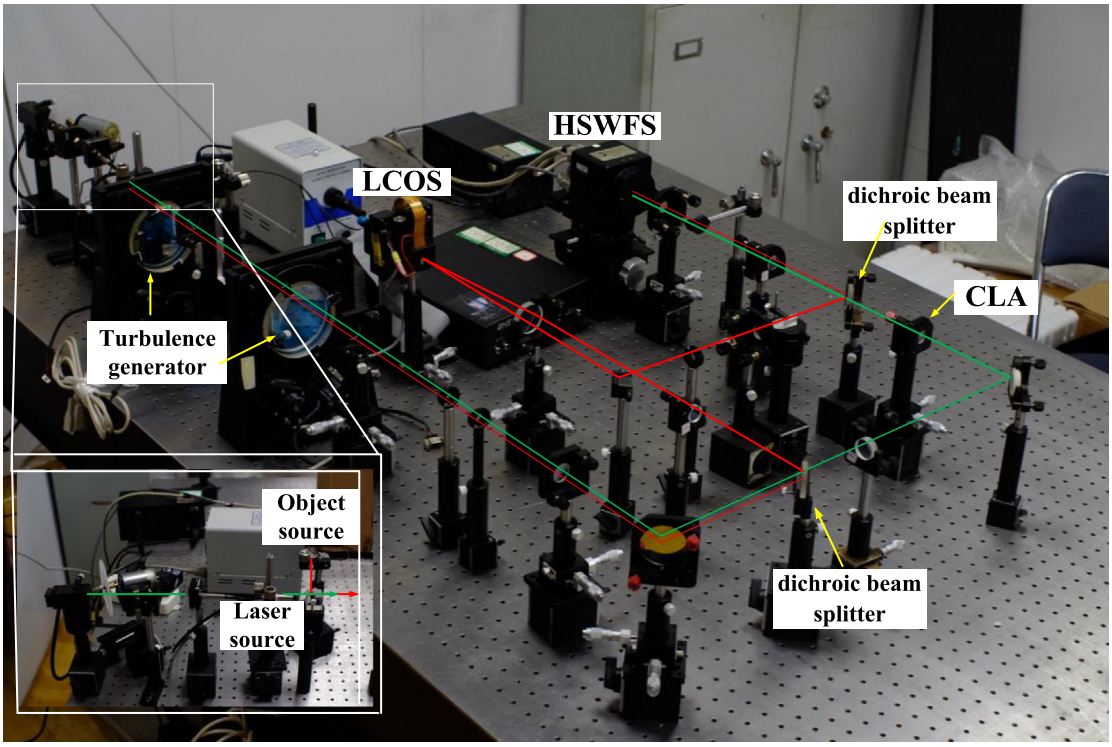

dichroic beam splitter

Fig. 8. Optical layout of the designed system. The light of object: 785 nm, and the laser: 532 nm.

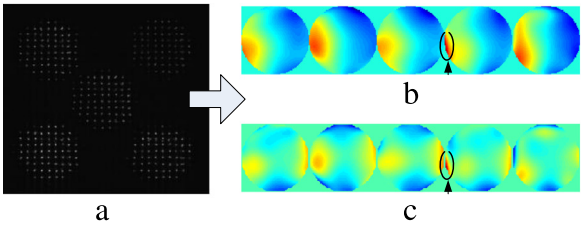

Fig. 9. The spots array and wavefronts of LGSs. (a) grabbed light spots array of five LGSs. (b) five wavefronts of LGSs. (c) LGSs' wavefronts without tip-tilts.

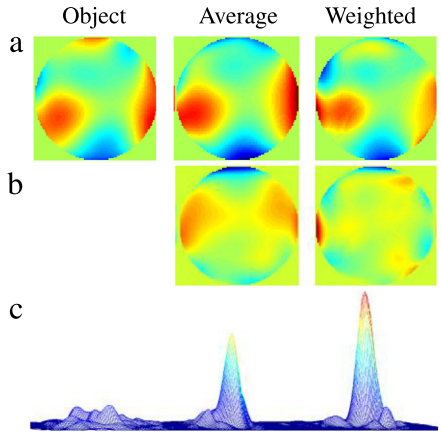

Fig. 10. Reconstructed wavefronts and correspondent PSF. (a) Reconstructed wavefronts; (b) residual wavefronts and (c) point spread function. Average method: residual wavefront, PV = 2.52 μm, RMS = 214.4 nm. SR = 0.25; Weighted method: residual wavefront, PV = 3.1 μm, RMS = 157.1 nm. SR = 0.41.

4.2. Solution of the focal shift

Using the low-altitude LGS would introduce the problem of pupil misrepresentation on wavefront corrector, which could not occur in any traditional AO system. The distance between LGS focus and the infinity one, defined focal shift, would be large for Rayleigh LGSs in Fig. 7. If this problem is not avoided, the footprint of the object and LGS beams will be of different size at the optical surface where are not conjugated to the telescope pupil. It will lead to a static aberration between object

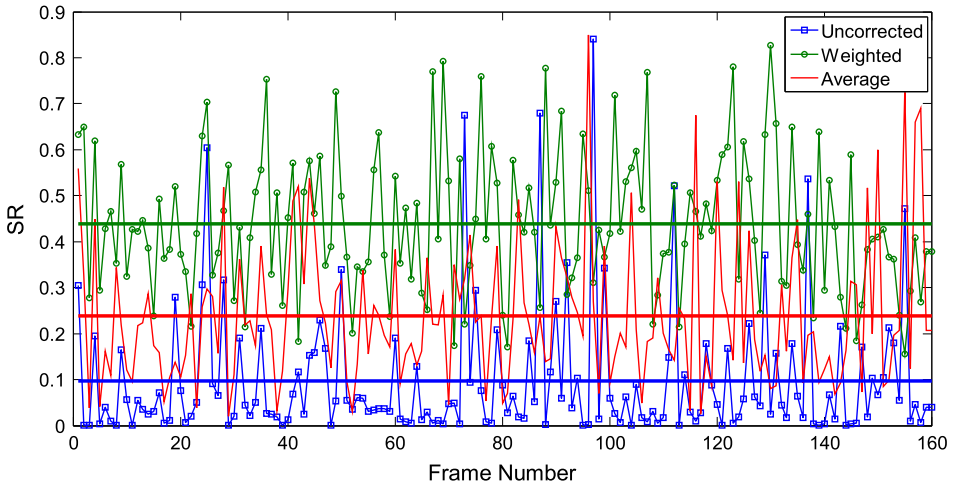

Fig. 11. Comparison of weighted method (green), average method (red) and uncorrected (blue). (For interpretation of the references to color in this figure legend, the reader is referred to the web version of this article.)

and LGS. Therefore, an open-loop system was designed and the object light and laser rays were separated and then combined. That is, different optical path is used for eliminating the focal shift as shown in Fig. 8.

4.3. The multi-LGS AO system in lab

The optical system is shown in Fig. 8. Light pass through relay lenses and then reach a dichroic beam splitter. The reflected part with wavelength larger than 700 nm will go to the object wavefront sensor branch consisting of a set of relay lenses, liquid crystal wavefront corrector (LCWFC), and Hartmann–Shark wavefront sensor (HSWFS). Additionally, laser beam which wavelength is 532 nm directly passes through the dichroic bean splitter to the LGSs wavefront sensor branch consisting of a set of relay lenses, collimating lens array (CLA) which is used to collimate five laser rays, and finally the HSWFS.

5. Experimental results and discussion

There is no any modulation on LCWFC during the verification experiment. Wavefronts of the object and LGSs were sensed at the same time by 100 subapertures, and then we compared the residual aberrations by subtracting the wavefront of object from wavefronts reconstructed by weighted method and average method. The grabbed light spots array from five LGSs were shown in Fig. 9(a). And five wavefronts from LGSs were shown in Fig. 9(b). Their wavefronts removed tip-tilts were listed in Fig. 9(c). In the experiment, some errors affect the reconstructed wavefront. There is a little defect on edge of CLA due to process, and it would influence the residual wavefront. The wavefront is reconstructed by Zernike modes of 35 and fitting error exists. The source of object and laser is bright enough, so the error of centroid measuring could be ignored. The results of reconstructed wavefronts, residual wavefronts and correspondent point spread function (PSF) were shown in Fig. 10. Taking the errors into account, the experiment basically agreed with the simulation.

In experiment, ϕ_4 was badly sensed in the area due to the defect of CLA as shown in Fig. 9. This leads to large wavefront reconstructed error, because the weighting factor of ϕ_4 is comparatively bigger than others in this area. Finally, the peak to valley (PV) of residual wavefront appears bigger. As for average method, such problem would be mitigated in the average. Because atmospheric turbulence changes randomly, so more than 150 frames of turbulence were used to test the weighted method. And the results were shown in Fig. 11. The average SR of uncorrected wavefront is about 0.1, and the SR is 0.22 with average method, and the SR is raised to 0.42 with weighted method. The experimental results agree with the simulation that the SR in center of FOV increase about 0.2 than average method.

6. Conclusions

In this paper, the weighted method for wavefront reconstruction is introduced in theory. In this method, different weighting factors were generated for different wavefronts of LGSs. The simulated result shows that our method could get a better correction within 2 arcmin FOV and at the center area of FOV the SR with weighted method improves about 0.2 than SR with average method and decreases with enlargement of FOV. As for extended object larger than isoplanatic region, our method could perform better. An experiment demonstrated weighted method could improve SR about 0.2 than average method at the center of FOV, which basically agree the simulation. The weighted method provides different weight factors according to the relative position of LGSs, so it requires wavefront sensed precisely where its weight factors are relatively large. The weighted method is simply and do not need the knowledge of C_n^2 profiles. And it shows promising applications in adaptive optics astronomical observations.

Acknowledgments

This work has been supported by state key laboratory of applied optics, Changchun institute of optics, fine mechanics and physics, Chinese academy of sciences, under the National Natural Science Foundation of China with grant numbers 11174274, 11174279, 61205021, 11204299, 61475152, 61405194.

References

[1] Q. Mu, Z. Cao, D. Li, L. Hu, L. Xuan, Open-loop correction of horizontal turbulence: system design and result, Opt. Express 47 (23) (2008) 4297–4301.
[2] Q. Mu, Z. Cao, L. Hu, Y. Liu, Z. Peng, L. Yao, L. Xuan, Open loop adaptive optics testbed on 2.16 m telescope with liquid crystal corrector, Opt. Commun. 285 (2012) 896–899.
[3] R. Ragazzoni, E. Marchetti, G. Valente, Adaptive-optics corrections available for the whole sky, Nature 403 (2000) 54–56.
[4] Martin J. Booth, Adaptive optical microscopy: the ongoing quest for a perfect image, Light: Sci. Appl. 3 (2014) e165.
[5] N. Meitav, E.N. Ribak, S. Shoham, Point spread function estimation from projected speckle illumination, Light: Sci. Appl. 5 (2016).
[6] Z. Zhang, Z. You, D. Chu, Fundamentals of phase-only liquid crystal on silicon (LCOS) devices, Light: Sci. Appl. 3 (2014) e213.
[7] John W. Hardy, Adaptive Optics for Astronomy Telescope, Oxford University Press, New York, 1998.
[8] P.L. Wizinowich, et al., The W.M. Keck Observatory laser guide star adaptive optics system: overview, Publ. Astron. Soc. Pac. 118 (2006) 297–309.
[9] C. Dainty, N. Ageorges, Laser Guide Star Adaptive Optics for Astronomy, NATO Scientific Affairs Division, London, 1997.
[10] Peter Wizinowich, Progress in laser guide star adaptive optics and lessons learned, Proc. SPIE (2012) 84470D–84470D-14.

[11] C. Baranec, et al., On-sky wide-field adaptive optics correction using multiple laser guide stars at the MMT, Astrophys. J. 693 (2) (2009) 1814–1820.
[12] C.B. Michael Lloyd-Hart, N. Mark Milton, Miguel, T.S. Snyder, J. Roger P. Angel, Experimental results of ground-layer and tomographic wavefront reconstruction from multiple laser guide stars, Opt. Express 14 (2006).
[13] Céline D'Orgeville, et al., Gemini South multi-conjugate adaptive optics (GeMS) laser guide star facility on-sky performance results, Proc. SPIE - Int. Soc. Opt. Eng. 8447.5 (2012) 491–497.
[14] Rigaut François, et al., Gemini multi-conjugate adaptive optics system review — I, Mon. Not. R. Astron. Soc. 437.3 (2013) 2361–2375.
[15] Benoit Neichel, et al., Gemini multi-conjugate adaptive optics system review II, Mon. Not. R. Astron. Soc. 440.2 (2014) 1002–1019.
[16] B.L. Roux, M. Langlois, M. Carbillet, et al., Ground layer adaptive optics for Dome C : optimization and performance, Adapt. Opt. (2007).
[17] A. Tokovinin, Seeing improvement with ground-layer adaptive optics, Publ. Astron. Soc. Pac. 116 (824) (2004) 941–951.
[18] Bin He, L.F. Hu, D.Y. Li, et al., A high precision phase reconstruction algorithm for multi-laser guide stars adaptive optics, Chin. Phys. B 25 (9) (2016).
[19] Dam, Marcos A. Van, A. H. Bouchez, B. A. Mcleod. Wide field adaptive optics correction for the GMT using natural guide stars, in: SPIE Astronomical Telescopes + Instrumentation 2014, 914813.